α-Synuclein perturbs *in vivo* neural activity following seeding in the olfactory bulb

Aishwarya S. Kulkarni[1], Maria del Mar Cortijo[1], Elizabeth R. Roberts[1], Tamara L. Suggs[1], Heather B. Stover[1], José I. Pena-Bravo[1], Jennifer A. Steiner[2], Kelvin C. Luk[3], Patrik Brundin[2], Daniel W. Wesson[1]

[1]Department of Pharmacology & Therapeutics
University of Florida
1200 Newell Dr.; Gainesville, FL, 32610, U.S.A.

[2]Center for Neurodegenerative Science, Van Andel Institute, Grand Rapids, MI, 49503, U.S.A.

[3]Department of Pathology and Laboratory Medicine, Center for Neurodegenerative Disease Research and Institute on Aging, University of Pennsylvania School of Medicine, Philadelphia, PA, 19104, USA.

*corresponding author: danielwesson@ufl.edu

RUNNING HEAD: *in vivo* physiology and α-Synuclein

Highlights:

- We investigated the influence of α-synuclein aggregate pathology on neural activity in the olfactory system of awake mice
- We injected pathogenic α-Syn fibrils into the olfactory bulb to recapitulate prodromal Parkinson's disease
- α-synuclein fibril injection influences beta and gamma band oscillatory activity
- Odor-evoked olfactory bulb activity is more vulnerable than that in piriform cortex to neuropathology triggered by α-synuclein fibril injections
- The influences on oscillations are not directly related to levels of α-synuclein assessed by immunostaining for pSer129-α-synuclein

Abstract

Parkinson's disease (PD) neuropathology is characterized by intraneuronal protein aggregates composed of misfolded α-Synuclein (α-Syn), as well as degeneration of substantia nigra dopamine neurons. Deficits in olfactory perception and aggregation of α-Syn in the olfactory bulb (OB) are observed during early stages of PD, and have been associated with the PD prodrome, before onset of the classic motor deficits. α-Syn fibrils injected into the OB of mice cause progressive propagation of α-Syn pathology throughout the olfactory system and are coupled to olfactory perceptual deficits. We hypothesized that accumulation of pathogenic α-Syn in the OB impairs neural activity in the olfactory system. To address this, we monitored spontaneous and odor-evoked local field potential dynamics in awake wild type mice simultaneously in the OB and piriform cortex (PCX) one, two, and three months following injection of pathogenic preformed α-Syn fibrils in the OB. We detected α-Syn pathology in both the OB and PCX. We also observed that the presence of α-Syn pathology, triggered by α-Syn fibril injection, influenced certain oscillatory spectral bands in these regions. These changes in neural activity occurred with region specificity, and in some cases transiently relative to the number of months that had elapsed after injection. Together, we provide evidence that α-Syn pathology in the olfactory system impacts *in vivo* neural activity and provides initial insights into its network-level effects.

Keywords: Parkinson's disease; Dementia; olfaction; synucleinopathy; Lewy pathology, piriform cortex; olfactory bulb; local field potential

Introduction

In addition to loss of substantia nigra dopamine neurons, a major pathological hallmark of Parkinson's disease (PD) is the presence of Lewy bodies and Lewy neurites, primarily composed of insoluble misfolded aggregates of α-Synuclein (α-Syn) (Goedert, 2001; Spillantini et al., 1997). Braak and colleagues (Braak et al., 2004, 2003a), suggested that in the early stages of PD pathogenesis, α-Syn aggregates accumulate in olfactory structures, including the olfactory bulb (OB), and the enteric nervous system before appearing in other brain regions. Interestingly, ~90% of individuals with PD exhibited olfactory deficits (Doty, 2012; Doty et al., 1988) prior to the onset of classic motor symptoms (Mahlknecht et al., 2015; Ross et al., 2008; Wu et al., 2011). Therefore, it is possible that pathogenic α-Syn aggregates within the olfactory system underlie the olfactory perceptual deficits observed in PD.

Recent studies in experimental animals have demonstrated that intracerebral inoculation of brain homogenates derived from mice and humans with synucleinopathy, or seeding recombinant pre-formed fibrils (PFFs) of α-Syn, triggers α-Syn pathology *in vivo* and *in vitro* (e.g., (Luk et al., 2012, 2009; Luk and Lee, 2014; Peelaerts et al., 2018; Rey et al., 2013). Injection of PFFs into the OB results in the spread of pathology between anatomically connected brain regions, including the piriform cortex (PCX) (Mason et al., 2016; Mezias et al., 2020; Rey et al., 2018a, 2016). Although the relationship between PD pathology and olfactory dysfunction are being explored clinically (Doty, 2017; Lee et al., 2014; Rey et al., 2018b; Wattendorf et al., 2009; Wen et al., 2017), the mechanisms underlying olfactory deficits in PD are unclear and animal modelling might provide insight into how neural processing is perturbed.

In both humans and rodent models, initial odor processing occurs in the OB where olfactory receptor neurons in the nasal epithelium synapse on OB glomeruli. Following local synaptic processing of this input (Schoppa and Urban, 2003; Wachowiak and Shipley, 2006) odor evoked information is then transferred to several secondary olfactory structures, including the PCX (Scott et al., 1980). As the primary region for processing odors, the OB is crucial for the basic initial aspects of olfaction, including the

fundamental ability to detect and recognize odors. Additionally, the PCX contributes to higher-order aspects of odor perception including odor learning (Gottfried, 2010; Wilson and Sullivan, 2011). Therefore, any perturbations in odor information processing through the local neural activity of the OB and/or the PCX could result in perceptual changes (Doucette et al., 2007; Nusser et al., 2001; Wilson, 2001). Thus, accumulation of α-Syn in the OB and PCX in persons with PD (Braak et al., 2003b; Doty, 2012) and olfactory deficits observed in PD (for review (Rey et al., 2018b)) led us to propose that pathogenic α-Syn perturbs olfactory neural activity.

Prior *in situ* and *ex vivo* studies have established that the natively unfolded form of α-Syn can modulate synaptic activity (Burré, 2015; Burré et al., 2010; Chandra et al., 2004). One study used brain surface electroencephalography to uncover changes in network activity of transgenic mice overexpressing human α-Syn (Morris et al., 2015). However, no studies to date have determined whether there are effects of pathogenic α-Syn assemblies on *local* neural activity *in vivo*. Here we use the olfactory system as a model to determine the influence of α-Syn aggregates on neural activity in awake animals. Specifically, we examined spontaneous and odor-evoked local field potentials (LFPs) within the OB and PCX of mice. LFPs reflect aggregate network activity (Buzsáki et al., 2012; Mitzdorf, 1985), and in the olfactory system, LFPs are comprised of three spectral bands, including theta (2-12 Hz), beta (15-35 Hz) and gamma (40-80 Hz). These bands are thought to play unique roles in the olfaction (Kay et al., 2009). Adding to their significance, beta and gamma oscillations in key basal ganglia structures are perturbed in PD (Burciu and Vaillancourt, 2018; Little and Brown, 2014; McCarthy et al., 2011).

Here we tested the hypothesis that accumulation of pathogenic α-Syn in the olfactory system leads to aberrant LFP activity. Through multi-site LFP recordings in awake mice following α-Syn PFF seeding in the OB, we found that α-Syn PFF seeding impairs olfactory oscillatory network activity. This suggests that synucleinopathy, and more specifically α-Syn aggregates in the olfactory system, might contribute to the olfactory deficits associated with early PD and the prodrome of the disease.

137

138

139 **Materials and Methods**

140 *Experimental subjects*

141 A schematic of the experimental timeline is displayed in **Figure 1**. A total of 57
142 female C57BL/6J mice (from donor stock originating at the Jackson Laboratory, Bar
143 Harbor, ME) were bred and maintained in a University of Florida, Gainesville, FL
144 vivarium. Mice were group housed until intra-cranial electrode implants as described
145 below, with food and water available *ad libitum*. All animal procedures were approved
146 by the University of Florida Institutional Animal Care and Use Committee and were
147 conducted in accordance with the guidelines of the National Research Council.

148

149 *Sonication and PFF handling*

150 Purified recombinant full-length mouse α-Syn (as described in Volpicelli-Daley et
151 al., 2014) was thawed at room temperature, and sonicated in a cup horn sonicator
152 (QSonica, Q700, Newton, CT) to yield short length PFFs (**Fig. 2**). During sonication
153 (amplitude of 50, process time of 3 mins with 1 s ON and 1 s OFF cycles), care was
154 made to ensure the sample was submerged in water, to ensure consistent sonication
155 power of the sample. Sonicated PFFs were stored at room temperature until being
156 microinjected into the brain as described below.

157

158 *Electron microscopy*

159 Electron microscopy was used to verify optimal PFF sonication in two separate
160 runs of PFF samples (**Fig. 2**) following the guidelines recommended by (Polinski et al.,
161 2018). The PFF samples from both runs were sonicated as described above. The
162 sonicated PFFs were then absorbed onto 400 mesh carbon coated grids (Electron
163 Microscopy Sciences, Hatfield, PA) and stained with 1% uranyl acetate for subsequent

164 electron microscopic imaging to confirm optimal sonication and thus fibril lengths. All
165 images were captured with a Tecnai G2 Spirit TWIN 120 kV transmission electron
166 microscope (FEI Company, Hillsboro, OR) equipped with an UltraScan 1000 (2k x 2k
167 resolution) CCD camera (Gatan Inc., Pleasanton, CA). Fibril lengths were measured in
168 Fiji Image J (Schindelin et al., 2012).

169

170 *Surgical procedures and animal care*

171 *OB microinjections*

172 We injected PFFs unilaterally in the OB of the mice no later than 3 hours after
173 sonication as described above. Briefly, mice were anaesthetized with isofluorane (~3%
174 in 1 l/min of O_2) and mounted in a stereotaxic frame accompanied with a water-filled
175 heating pad in order to maintain body temperature (38°C). Marcaine (1.7 mg/ml, s.c.;
176 Hospira Inc., Lake Forest, IL) was injected into the site of the future wound margin. The
177 analgesic meloxicam was also provided s.c. (5 mg/ml; Putney Inc, Overland Park, KS),
178 and following, a midline incision was made to expose the skull cap. Next, a craniotomy
179 (~0.5 mm) was drilled in order to access the right OB (5.4 mm anterior to bregma, 0.75
180 mm lateral) and injected with either 800 nl of sterile PBS (pH 7.4; Gibco, Fisher
181 Scientific, Hampton, NH) or 800 nl of sonicated PFFs using a glass micropipette at 2
182 nl/sec (1 mm ventral in the OB). Following the injection, and a resting period of 3 mins,
183 the micropipette was gently withdrawn from the injection site at a rate of 200 μm / min.
184 Following injections, the mice from all cohorts received *ad libitum* access to food and
185 water, and were allowed to recover on a heating pad for at least 8 hrs.

186

187 *Implantation of LFP electrodes*

188 Following injection of PFFs, and either 1, 2, or 3 months follow up periods, all
189 mice were again sedated and prepared for cranial surgery as outlined above; this
190 surgery included implantation of two pairs of twisted teflon-coated stainless steel bipolar
191 electrodes (catalog # 791500, 0.005" diameter; A-M systems, Carlsborg, WA). The

192 electrodes were implanted ipsilaterally to the PFF injection into both the OB and PCX.
193 The OB coordinates were 3.8 mm anterior from bregma, 1 mm lateral, 1 mm ventral and
194 the PCX coordinates were 0 mm bregma, 3.4 mm lateral, and 4 mm ventral. A third
195 craniotomy was drilled over the contralateral cortex for the placement of a single
196 stainless steel electrode to serve as the ground (catalog # 792900, 0.008" diameter, A-
197 M Systems). This assembly was then cemented onto the skull along with a small plastic
198 head-bar for subsequent head-fixation as defined below. After surgery, the mice were
199 singly housed and allowed to recover on a heating pad for at least 8 hrs. These
200 implanted mice had *ad libitum access* to food, water, and received subcutaneous
201 meloxicam daily for 3 days (5 mg/kg).

202

203 *Outline of experimental groups*

204 Mice were pseudorandomly divided into two treatment groups (*i.e.,* PBS or PFF
205 treated) and aged for 3 different durations post injection (1, 2, or 3 months). All mice
206 were injected at 2-3 months of age (mean age upon injection: 64 ± 1.5 days (mean ±
207 SEM)). Total animals aged per group include PBS: 1 (*n*= 9), 2 (*n*=10), or 3 (*n*=8) months
208 post injection and PFF: 1 (*n*= 8), 2 (*n*=10), or 3 (*n*=12) months post injection.

209

210 *Awake LFP recordings and data acquisition*

211 We recorded spontaneous and odor-evoked LFP activity from 17 mice at 1
212 month post injection (*n*= 9 PBS, *n*= 8 PFF), 20 mice at 2 months post injection (*n*= 10
213 PBS, *n*= 10 PFF), and 20 mice at 3 months post injection (*n*= 8 PBS, *n*= 12 PFF).
214 During any given day, mice of more than one condition [1, 2, or 3 months post injection
215 and/or PBS/PFF treatment group] were used in recordings. A schematic of the
216 recording session structure is shown in **Figures 3A & 3B**. All the recordings were
217 performed in a dimly-lit, well-ventilated room maintained at 20-22°C, between 0900 and
218 1800 hrs.

219 Mice were head-fixed and an odor-port was positioned ~2 cm from the nose,
220 prior to the start of the recordings, as we have described previously (Gadziola et al.,
221 2015). To monitor spontaneous LFP activity, we allowed the animal to rest during head-
222 fixation for several minutes (~5 mins) prior to and following a series of odor deliveries
223 (**Fig. 3B**). All odors and the blank stimulus (mineral oil) were presented for 4 secs each,
224 in a pseudorandom order, with an approximately 15 secs inter-stimulus interval.
225 Throughout recordings, OB and PCX activity was acquired at 2 kHz and filtered (100
226 Hz, 2nd order low-pass, 60 Hz notch) along with stimulus presentation events using a
227 Tucker Davis Technologies RZ5D amplifier (Alachua, FL).

228

229 *Stimulus delivery*

230 For odor presentation, odors including isopentyl acetate, 2-butanone, and 1,7-
231 octadiene (Sigma Aldrich, St. Louis, MO) were each diluted in their liquid state to
232 133.332 Pa (1 Torr) and 266.645 Pa (2 Torr) in light mineral oil (Sigma Aldrich) which
233 also served as the blank stimulus. Stimulus vapors controlled with an air-dilution
234 olfactometer were run from glass headspace vials (100 ml/min) where they were later
235 blended with clean nitrogen (900 ml/min) in the odor port thereby yielding a total odor
236 flow rate of 1 L/min. The olfactometer was equipped with independent stimulus lines up
237 to the point of entry into a Teflon odor port, in order to eliminate chances of cross-
238 contamination of the stimuli and also to allow for rapid temporal control of odor
239 dynamics as they reach the animal. To confirm the dynamics of the odor plume as it
240 leaves the odor port, we used a photoionization detector (Aurora Scientific, Aurora CO).
241 As shown in **Figure 3C**, odor delivery occurred rapidly, and was largely stable
242 throughout the 4 sec of delivery.

243

244 *Tissue collection and histology*

245 Within 48 hrs after recordings, the mice were overdosed with Fatal-plus (0.01
246 ml/g; Vortech Pharmaceutical Ltd, Dearborn, MI). Following confirmation of deep
247 sedation, they were perfused with cold saline and subsequently 10% phosphate

248 buffered formalin. Brains were collected and stored at 4 ºC in 10% formalin / 30%
249 sucrose prior to sectioning. Serial 40 µm thick coronal sections were collected using a
250 sliding microtome, and stored in Tris-buffered saline (TBS, pH 7.4) with 0.03% sodium
251 azide. These sections were used for electrode verification and phosphoserine 129
252 (Pser129) immunofluorescence.

253

254 *Pser129 immunofluorescence*

255 Presence of Pser129 α-Syn-immunopositive inclusions is considered
256 pathological given the abundance of this post-translationally modified form of α-Syn in
257 Lewy pathology (Fujiwara et al., 2002). Our previous work has also shown that Pser129
258 α-Syn-immunopositive inclusions in the animal model we used in the present study are
259 positive for ubiquitin, p62, Thioflavin S and are Proteinase K resistant, all features of
260 clinical Lewy pathology (Rey et al., 2016). Thus, we used Pser129 immunofluorescence
261 to quantify pathological burden resultant from OB PFF microinjections. OB and PCX
262 sections floating in deionized water were rinsed thrice in TBS and dilution buffer (10
263 mins each). Next, the sections were blocked in 20% normal donkey serum in TBS for 20
264 mins and incubated for 24 hrs in primary antibody rabbit anti-Pser129 (1:5000 in dilution
265 buffer, catalog # EP1536Y, Abcam, Cambridge, MA) at room temperature. On the
266 following day, all sections were rinsed four times in dilution buffer (10 mins) and
267 incubated for 2 hrs in secondary antibody Alexa Fluor 594 goat anti-rabbit IgG (1:500 in
268 dilution buffer, catalog # A11012, Invitrogen, Carlsbad, CA). Sections were rinsed thrice
269 in TBS and twice in double distilled water (5 mins each). Finally, tissue was placed on
270 slides and cover-slipped with mounting media containing DAPI (Fluoromount-G; 4',6-
271 diamidino-2-phenylindole; Invitrogen). All immunofluorescence runs contained tissue
272 from more than one age and treatment group.

273

274 *Electrode verification*

275 PCX electrode tips/recording sites were verified with microscopy. Due to the
276 ease of targeting, not all mice used in the study underwent exclusive examination for

electrode tip placement in the OB. For PCX recording site verification, tissue processed for anti-Pser129 immunofluorescence (counterstained with DAPI) was used. When additional sections were needed for confirmation of recording sites, additional PCX tissue was placed on slides and counter-stained with DAPI. Only one mouse (PBS, 2 months post injection) did not contribute PCX data since the electrode was misplaced. The total numbers of animals contributing data / brain region is defined below.

Pser129 imaging and quantification

The OB and PCX were identified based on an established brain atlas (Paxinos and Franklin, 2000). Images of the OB and PCX were acquired from the hemisphere ipsilateral (identified from the electrode tracks) to the OB microinjection. All the imaging was performed with a Nikon Ti2e microscope equipped with a 15MP monochrome camera and using 20X magnification. Additionally, image acquisition settings, particularly the gain, light intensity, and exposure were kept constant for all images. First, images were collected which included the OB and PCX (≥4 images/region). Attempts were made to acquire images from similar anterior-posterior extents of each brain area. Next, the images were cropped so that the resultant image included solely OB and PCX, and that the images spanned the majority of cell layers, as exemplified in **Figure 4**. These cropped images were thresholded using fixed settings across all images for later quantification of Pser129 levels. The % area in each of the cropped and thresholded images occupied by Pser129 was then calculated as a ratio of the total pixel area : the pixel area above threshold.

Analysis and Statistics

In total, we acquired spontaneous and odor-evoked LFP activity from 17 mice at 1 month post injection (n= 9 PBS, n= 8 PFF), 20 mice at 2 months post injection (n= 9 PBS, n= 10 PFF), and 20 mice at 3 months post injection (n= 8 PBS, n= 12 PFF). All of these mice contributed clean artifact free signals and also passed the electrode placement confirmation described above.

306 Analysis of the LFP data was performed in Spike 2 (Cambridge Electronic
307 Design, Milton, Cambridge). Data were processed using Fast Fourier Transform (FFT)
308 analysis [for spontaneous (1.006 secs Hanning window and 0.994 Hz resolution) and
309 odor evoked (0.503 sec Hanning window and 1.987 Hz resolution)] in order to classify
310 and distribute the data within different LFP frequency bands. Power spectra of
311 spontaneous and odor-evoked LFP activity were extracted from 0-100 Hz. LFP spectral
312 bands were defined as theta (1-10 Hz), beta (10-35 Hz), and gamma (40-70 Hz) (Kay et
313 al., 2009). OB-PCX spontaneous LFP activity was analyzed over a duration of 200 secs
314 sampled both prior to and following presentation of odors (at the start and end of the
315 recording session respectively). Odor-evoked response magnitude was used as a
316 variable to measure odor-evoked LFP activity. OB-PCX odor-evoked response
317 magnitude is a ratio of time matched (4 secs) LFP power during odor presentation to
318 LFP power before odor presentation. Herein we focus our odor-evoked analyses solely
319 on 1 Torr isopentyl acetate trials. This is based upon the inconsistent responses elicited
320 by 2-butanone and 1,7-octadiene in all mice, including those PBS treated. Further,
321 when collapsing across groups, we did not find an effect of 1 Torr versus 2 Torr intensity
322 of isopentyl acetate and so for simplicity we restrict all analyses to 1 Torr isopentyl
323 acetate.

324 All statistical analyses were performed using Microsoft Excel and Graphpad
325 Prism 8 (San Diego, CA). Any comparison between PFF and PBS injected mice aged
326 for 1, 2, or 3 months post injection was conducted using repeated measures ANOVA
327 and 2-way ANOVA. For post-hoc analyses, either Tukey's multiple comparison tests or
328 *t*-tests were used.

329

330

331 **Results**

332 *Accumulation of Pser129 pathology in key olfactory structures following OB α-Syn*
333 *seeding.*

334 To induce α-synucleinopathy in the olfactory system, PFFs or PBS as a control,
335 were unilaterally injected into the OB of 2-3 months-old female mice. The mice were
336 then allowed to age for either 1, 2, or 3 months prior to being implanted with electrodes
337 into their OB and PCX, ipsilateral to the injection, and LFP recordings performed (**Fig.**
338 **1**) as described below. Following recordings, the brains were collected and processed
339 for anti-Pser129 immunofluorescence. Confirming previous results using this OB PFF
340 seeding model (Rey et al., 2018a, 2016), we observed Pser129 burden in key olfactory
341 structures, including the OB itself and the PCX (**Fig. 4**). Across all groups, there was an
342 effect of brain region on Pser129 levels ($F(2, 33) = 9.586$, $p = 0.0005$). Post hoc tests
343 revealed that the PCX ($t = 2.002$, $p = 0.00002$) was vulnerable to pathological
344 accumulation of misfolded α-Syn as indicated by the higher level of burden. In contrast,
345 and in agreement with previous work (Rey et al., 2016), the OB did not possess high
346 levels of burden across any group (**Figs. 4B & 4C**). Instead, low levels of Pser129
347 burden was detected in the OB, which we observed to be spanning the layers of the OB
348 (with the injection targeted to the inner layers). Pser129 burden was also observed
349 throughout all 3 cell layers of the PCX (**Fig. 4B**).

350

351 *Preservation of spontaneous LFP dynamics following α-Syn seeding.*

352 We began our investigation into the influence of α-Syn aggregates on LFP
353 dynamics by analyzing spontaneous (*viz.,* those in the absence of experimentally-
354 applied odors) levels of theta, beta, and gamma-band powers in the OB and PCX of
355 mice aged 1, 2, or 3 months post injection (the same mice used for histology above). As
356 is well established (for review (Kay et al., 2009)), spontaneous OB and PCX LFP activity
357 is characterized by prominent theta band power coupled with respiratory cycles, along
358 with beta and also some gamma band powers which also occur in somewhat phasic
359 manners with respiratory theta (**Fig. 5A & 5B**).

360 The most fundamental aspects of OB activity, how it operates during
361 spontaneous states, was intact following PFF injection. We did not find an overall
362 (across age groups) change in theta ($F(1,51) = 0.993$, $p = 0.324$), beta ($F(1,51 = 0.035$,

363 p = 0.853), or gamma band powers (F(1,51) = 0.013, p = 0.910) in the OB when
364 comparing PBS injected animals to those injected with PFFs (**Fig. 6**). Post-hoc tests
365 within these spectral bands, and also within individual age groups, similarly did not
366 reveal an effect of PFF treatment (p > 0.05, 2-tailed paired t-tests).

367 Next, we performed similar analyses of spontaneous LFPs in the PCX. While in
368 the PCX we similarly did not find an overall change in theta (F(1, 50) = 0.017**,** p =
369 0.897), beta (F(1, 50) = 0.084**,** p = 0.774), or gamma band power (F(1, 50) = 0.073, p =
370 0.788) when comparing PBS animals to those injected with PFFs (**Fig. 6**), there were
371 significant differences between PFF and PBS animals. These were observed in both the
372 beta (t = 2.110, df = 17, p = 0.018; 2-tailed paired t-test) and gamma band powers (t =
373 2.228, df = 10, p = 0.038, 2-tailed paired t-test) in the 2 months post injection groups
374 (**Fig. 6**) with PFF-treated animals displaying elevations in the power of both bands.
375 Thus, despite pathogenic propagation of α-Syn from the seeded structure (the OB) into
376 a monosynaptically interconnected structure (the PCX), these systems (*i.e.,* their
377 networks) were not similarly vulnerable to the influence of α-Syn. This highlights that the
378 PCX may be more vulnerable than the OB to α-Syn influences on spontaneous activity.

379

380 *α-Syn seeding results in heightened OB beta-band odor-evoked activity.*

381 The OB and PCX are important for the formation of olfactory perception, and the
382 processing of odor information in each of these stages is considered critical for
383 olfaction. Odor-input drives increases in both beta and gamma-band power activity in
384 the OB (Kay et al., 2009). Beta band power is especially considered important for the
385 coordinated transfer of sensory information between brain regions (Haegens and Zion
386 Golumbic, 2018; Kopell et al., 2000) and thus any changes in beta activity during odor
387 may be especially influential to perception. Therefore, we next took advantage of the
388 monosynaptic and bisynaptic inputs of odor information into these structures by
389 analyzing odor-evoked LFPs (**Fig. 7A**) and how OB PFF seeding may impact odor-
390 evoked activity. We compared the LFP spectral power during 4 secs of odor (1 Torr
391 isopentyl acetate) versus the 4 secs immediately prior to odor (**Fig. 7B**) to calculate an

odor-evoked power ratio. We then averaged this across all trials in the session (4-5 trials/animal) to calculate average odor-evoked power ratios as a simple measure of odor-evoked network activity.

In the OB, while analyses of odor-evoked power ratios did not uncover an effect in either the theta ($F(1, 50) = 0.944$, $p = 0.336$) or gamma bands ($F(1, 50) = 0.389$, $p = 0.536$), there was a significant effect of PFF treatment increasing odor-evoked beta band activity ($F(1, 50) = 5.531$, $p = 0.023$) (**Fig. 8**). Post-hoc tests within these spectral bands, and also within individual age groups, similarly did not reveal an effect of PFF treatment ($p>0.05$, 2-tailed paired *t*-tests). Nevertheless, there is a clear elevation in beta-band odor evoked power ratios in the PFF-treated animals across all three age groups.

In contrast to the OB, theta ($F(1, 49) = 1.351$, $p = 0.251$), beta ($F(1, 49) = 0.042$, $p = 0.839$), and gamma band odor evoked powers ($F(1, 49) = 3.380$, $p = 0.072$) were similar between PBS and PFF treated animals across all ages in the PCX (**Fig. 8**). This indicates that, at least at the level of LFP monitoring, the effect of α-Syn OB seeding is most dramatic in shaping OB odor-evoked activity. This is a significant finding since the OB provides nasal-derived odor information into the entirety of down-stream brain regions.

Are oscillatory dynamics correlated with Pser129 levels?

Finally, we sought to test whether the levels of local Pser129 within either the OB or PCX may be correlated with the changes in oscillatory dynamics. The effect on spontaneous LFP dynamics at 2, but not 1 or 3 months of age post injection indicates a transient change in network dynamics which does not evidently/directly coincide with the levels of Pser129 progression observed in the PCX over time (**Fig. 6**). As a population across all animals, indeed no significant correlation existed between levels of Pser129 and spontaneous LFP power within the 2 months beta ($r(8) = -0.019$, $p = 0.959$) or gamma band activity ($r(8) = -0.125$, $p = 0.731$) in the PCX (**Fig. 9A**).

Our analysis of odor-evoked activity demonstrated significantly elevated levels of beta-band activity following PFF injection (**Fig. 8**). Further, some PFF-treated animals contributed abnormally high levels of odor-evoked beta-band activity (**Fig. 8**). Upon post-hoc inspection, we determined that some of these mice were also those which displayed elevated Pser129 pathological burden in the olfactory system led us to predict these factors were related. That said, as a population across all animals, no significant correlation existed between levels of Pser129 and odor-evoked power ratios within beta activity in the OB ($r(28) = 0.319$, $p = 0.086$) (**Fig. 9B**). Taken together, neither of two major effects observed in PFF seeded mice, including elevations in OB odor-evoked beta power and elevations in spontaneous PCX beta and gamma band powers, were correlated with levels of pSer129 pathology in these respective structures.

Discussion

We tested the hypothesis that progressive development of α-Syn aggregates in the olfactory system impacts neural dynamics. While key regions within the basal ganglia system display aberrant synchrony of neural dynamics which may contribute to motor deficits in PD (Brown and Williams, 2005; De Hemptinne et al., 2015; Hammond et al., 2007; Kühn et al., 2006; Moran et al., 2008), the direct contributions of α-Syn aggregates to neural dynamics *in vivo* are unresolved. This is an important question because hyposmia is prevalent in PD, and often develops before the onset of clear motor deficits. Furthermore, greater insight into the impact of α-Syn aggregates on neural circuits is important for our understanding of functional deficits in PD and related synucleinopathies. Perturbations in neural synchrony might be highly relevant to the symptomology of clinical synucleinopathies since they may alter key aspects of function, from cognitive, motor, to sensory – depending upon the system impaired.

We used α-Syn seeding in mice in combination with olfactory LFP recordings. The olfactory system is an excellent model to test whether pathogenic α-Syn impacts neural dynamics, given both the known aggregation of Lewy bodies in the OB during the

earliest states of PD, and decades of work carefully examining the dynamics of LFPs in the OB and PCX, including how these dynamics are influenced by odors. Importantly, LFPs are reflective of aggregated network activity (Buzsáki et al., 2012; Mitzdorf, 1985) and are considered a substrate for the rhythmic sampling of sensory information (Haegens and Zion Golumbic, 2018). Therefore, changes in LFPs may impact odor perception. Here we found that the progressive development of α-Syn aggregates influenced specific LFP spectral bands, and did so in region-specific manners (*viz.,* not all brains regions were equally vulnerable), and in some cases transiently relative to the amount of time following seeding.

Reconciling Pser129 pathology with that of previous studies.

The OB seeding model we used is associated with impaired odor perception, yet spared motor function (Rey et al., 2016). We found, as expected, that injection of α-Syn PFFs into one OB triggered α-Syn accumulation of intraneuronal Pser129 immunoreactive aggregates in inter-connected olfactory structures, particularly in the PCX **(Fig. 4)** which has dense reciprocal connection with the OB. Based on prior studies demonstrating Pser129 immunoreactivity in olfactory brain regions of mice following PFF injections (Rey et al., 2018a, 2016), we interpret the Pser129 immunofluorescence we observe in the PCX as being the consequence of seeding of endogenous α-Syn. The uptake pattern we observed is similar to that previously reported (Rey et al., 2016, 2013). Herein and in our earlier studies (Rey et al., 2018a, 2016), injection of PFFs into the OB resulted in elevations in Pser129 relative to the time following seeding. While there was no elevation over time of Pser129 staining in the OB itself, the PCX did show subtle increases in pathology from 1 to 3 months of age, albeit not significant. Also similar to our earlier studies (Rey et al., 2016, 2013), we found significantly greater levels of Pser129 in the PCX than the OB.

α-Syn *PFF injection influences beta and gamma band activities.*

477 Monitoring the spontaneous and odor-evoked LFP activities simultaneously in
478 both the OB and PCX revealed elevations in beta and gamma-band powers in mice with
479 Pser129-positive aggregates. There are several points worthy of discussion in this
480 regard, which we organize by oscillatory band:

481 *Theta band activity*

482 First, no changes were found in theta-band power, which is a prominent
483 oscillatory power observed in both the OB and PCX. Theta oscillations in the OB are
484 generated by intranasal afferent input, and OB and PCX theta cycles are often coupled
485 to respiration (Kay et al., 2009; Kay and Stopfer, 2006; Komisaruk, 1970). The spared
486 theta power observed herein suggests that OB α-Syn pathology did not overtly alter the
487 basic sensory-motor functions impacting the olfactory system (*i.e.,* respiration).

488 *Beta band activity*

489 Our results indicate that α-Syn aggregates, seeded by PFF injection into the OB,
490 can generate PD-relevant elevations in beta band activity during both spontaneous **(Fig.**
491 **6)** and odor-evoked **(Fig. 8)** states. Beta oscillations reflect large-scale activity between
492 interconnected structures (Kopell et al., 2000; Spitzer and Haegens, 2017) such as that
493 between the OB and PCX (Kay and Beshel, 2010; Neville and Haberly, 2003).

494 The changes we uncovered in beta activity are especially relevant to PD
495 pathophysiology. Striatal and cortical beta band activity is elevated in persons with PD
496 and deep brain stimulation, levodopa, and anti-cholinergic treatment may act by means
497 of suppressing elevated beta power in the cortico-basal ganglia loop (Brown, 2006;
498 Brown et al., 2001; Eisinger et al., 2020; Giannicola et al., 2010; Little and Brown, 2014;
499 McCarthy et al., 2011). Additionally, deep brain stimulation of the subthalamic nucleus
500 was shown in one study to improve cortical function in PD and reduce the excessive
501 beta phase coupling of motor cortex neurons (De Hemptinne et al., 2015). Differences
502 in beta band activity are proposed to be a network determinant of PD pathophysiology
503 (Feingold et al., 2015). Our results indicate an important role for α-Syn related
504 pathologies in these clinical pathophysiologies.

505 Notably, beta oscillations increase depending upon sensory and cognitive
506 demands (Bauer et al., 2006; Spitzer et al., 2010; Spitzer and Haegens, 2017; van Ede
507 et al., 2010) and in the olfactory system beta oscillations are considered especially
508 involved in odor learning (Gervais et al., 2007; Lowry and Kay, 2007; Martin et al.,
509 2007). In our study, while the mice were awake while being delivered odors, they were
510 not engaged in a cognitively demanding task. Interestingly, in our previous work, which
511 uncovered progressive olfactory perceptual deficits following injection of PFFs into the
512 OB (Rey et al., 2016), we used a task which relies partly upon working memory. Based
513 on these observations in our animal model, we propose that aberrant OB odor-evoked
514 beta-band activity can perturb odor perception in manners which may underlie the
515 impacts of PFF seeding on odor perception (Rey et al., 2016).

516 *Gamma band activity*

517 Our results indicate that α-Syn aggregates in olfactory nuclei are associated with
518 elevated levels of spontaneous gamma band activity in the PCX **(Fig. 6)**. Reciprocal
519 dendodendritic activity between OB granule and mitral / tufted cells generates gamma
520 band activity (Shepherd, 1972). Odor-evoked OB gamma oscillations reflect the local
521 network activity within the OB and PCX with gamma in the PCX considered to originate
522 locally (Neville and Haberly, 2003; Rall and Shepherd, 1968). This implies that while the
523 PFFs may have seeded in one structure (in this case, the OB), they may yield their
524 greatest influence upon interconnected structures which hold connectivity with the OB
525 (like the PCX).

526

527 *Some brain networks may be more vulnerable to the influence of α-Syn PFF injections*
528 *than others.*

529 Our two main effects of α-Syn PFF injections were localized to either the OB or
530 PCX, but *not* to both. Indeed, we uncovered that despite pathogenic propagation of α-
531 Syn from the seeded structure (the OB) into a monosynaptically interconnected
532 structure (the PCX), these structures (*i.e.,* their networks) were not similarly vulnerable
533 to the influence of α-Syn. For instance, a striking effect in PFF seeded mice was an

534 elevation in odor-evoked beta power (**Fig. 7 & 8**). This was observed only in the OB –
535 suggesting that the OB is either directly impacted by α-Syn pathology, or, that the PCX
536 which is known to innervate the OB and influence local inhibition, is impacted and this
537 results in elevated beta power during odor inhalation. We propose the latter model is at
538 play. This is based upon the known nature of beta activity to be
539 originating/communicating between brain regions and also the notably low levels of
540 Pser129 in the OB compared to the PCX. Regardless of mechanism, the results of the
541 odor-evoked analyses highlight that the impact of α-Syn aggregates may be region
542 specific.

543 Similarly supporting this case, monitoring the spontaneous LFP activity
544 simultaneously in both the OB and PCX revealed elevations in beta and gamma-band
545 powers. Interestingly, in these measures of spontaneous activity, only the PCX, not also
546 the OB, was perturbed (**Fig. 5 & 6**). As introduced above, gamma-band activity is
547 resultant from network interactions within a local population of neurons and thus the
548 finding that the OB also did not display changes in spontaneous LFPs, not even
549 gamma-band activity, suggest that the PCX may be more vulnerable than the OB to α-
550 Syn influences on spontaneous activity.

551 In our model, α-Syn aggregates are present within several processing stages of
552 the olfactory system (OB, AON, and PCX). Therefore, we cannot determine with
553 certainty in which neuronal populations (single or multiple) that the α-Syn aggregates
554 influence neural activity, which ultimately give rise to the altered LFPs we detect in the
555 OB and PCX.

556

557 *The influence of α-Syn PFF injection on oscillations is not directly related to levels of*
558 *pSer129.*

559 Neither of two major effects observed in PFF injected mice, including elevations
560 in OB odor-evoked beta power (**Fig. 7 & 8**) and elevations in spontaneous PCX beta
561 and gamma band powers (**Fig. 5 & 6**), were correlated with levels of pSer129 pathology
562 in the respective structures (**Fig. 9**). In the case of the elevations in PCX spontaneous

563 power, these were only observed 'transiently', in the two, but not the one or three-
564 months post-injection groups (**Fig. 6**). This transient occurrence is striking since
565 pSer129 pathology in the PCX increased with age (**Fig. 4C**). Further, the transient effect
566 implies that neural networks are more vulnerable to α-Syn pathology at a certain time-
567 point following injection of α-Syn PFFs. Adding to this, the elevations in beta power in
568 the OB during odor were stable regardless of delay post seeding (**Fig. 7 & 8**) which had
569 no impact on pSer129 levels in the OB (**Fig. 4C**).

570 Cell culture and slice physiology studies demonstrated that pathological α-Syn
571 perturbs normal synaptic function (Volpicelli-Daley et al., 2011; Wu et al., 2019), for
572 instance, by oligomeric α-Syn's actions upon glutamatergic receptors (Durante et al.,
573 2019). Further, brain-surface electroencephalography from transgenic mice
574 overexpressing human α-synuclein, throughout the brain, uncovered aberrant activity,
575 including epileptiform events (Morris et al., 2015). Our *in vivo* results suggest that
576 elevations in pathological α-Syn, up to a particular level, may be sufficient to entail
577 changes in synaptic coupling or perhaps efficacy which may result in the aberrant LFP
578 activity. While we do not elucidate the precise cellular mechanism whereby α-Syn
579 seeding perturbed neural activity, our correlation results do indicate that function is not
580 strongly correlated with pathogenic α-Syn levels at least at the level of the local
581 networks (*viz.,* detectable with LFPs). This outcome points towards the likely influential
582 role of other pathologies related to α-Syn aggregates in shaping neural dynamics in the
583 context of PD. For instance, α-Syn aggregates accumulate in axons where they likely
584 cause degeneration of the axons as well as dendrites (Volpicelli-Daley et al., 2011).
585 Thus, it is possible that the influence of α-Syn aggregates on neural activity would be
586 more directly correlated with changes in activity as the aggregates mature.

587

588 *Conclusions.*

589 Our results extend important mechanistic work performed in cell culture and in brain
590 slices indicating that α-Syn aggregates can perturb synaptic activity. Thus, we used
591 awake mice and studied how progressive changes in α-Syn aggregate pathology affects

592 the olfactory system at the network level. We found changes in neural activity that were
593 region-specific, but did not directly correlate to the local degree of α-Syn aggregate
594 pathology. Future work to assess levels of other pathologies along with simultaneous
595 neural recordings will be informative, as will be work utilizing methods allowing for
596 monitoring the activity of select cell populations to understand the cell types specifically
597 vulnerable to the effects of synucleinopathy.

598

599

600

601

602

603

604

605

606

607

608

609

610

611

612

613

614

615

Acknowledgements: Research reported in this publication was supported by the National Institute on Deafness and Other Communication Disorders of the National Institutes of Health under Award Numbers R01DC016519 (D.W and P.B.) and R01DC014443 (D.W.). The content is solely the responsibility of the authors and does not necessarily represent the official views of the National Institutes of Health. We acknowledge the Van Andel Research Institute and many individuals and corporations that financially support research into neurodegenerative disease at Van Andel Research Institute. We also thank the Udall Center for Parkinson's Research at the University of Pennsylvania for generously providing α-Syn PFFs and Karen Kelley at the University of Florida Interdisciplinary Center for Biotechnology Research for expert advice and training in electron microscopy.

Competing interests: P.B. has received commercial support as a consultant from Axial Biotherapeutics, CuraSen, Fujifilm-Cellular Dynamics International, IOS Press Partners, LifeSci Capital LLC, Lundbeck A/S and Living Cell Technologies LTD. He has received commercial support for grants/research from Lundbeck A/S and Roche. He has ownership interests in Acousort AB and Axial Biotherapeutics and is on the steering committee of the NILO-PD trial. The authors declare no additional competing financial interests.

Author contributions: Investigation (A.K., E.R., J.P-B, H.S., M.C.), Formal analyses (A.K., E.R., T.S.), Validation (A.K., T.S., D.W.), Methodology and Resources (J.A.S., K.C.L, and D.W.), Writing-Original draft (A.K.), Review and Editing (A.K., J.A,S., P.B., D.W.), Conceptualization, Supervision, and Funding acquisition (P.B. and D.W.)

References

Bauer, M., Oostenveld, R., Peeters, M., Fries, P., 2006. Tactile spatial attention enhances gamma-band activity in somatosensory cortex and reduces low-frequency activity in parieto-occipital areas. J. Neurosci. 26, 490–501. https://doi.org/10.1523/JNEUROSCI.5228-04.2006

Braak, H., Ghebremedhin, E., Rüb, U., Bratzke, H., Tredici, K., 2004. Stages in the development of Parkinson's disease-related pathology. Cell Tissue Res 318, 121–134. https://doi.org/10.1007/s00441-004-0956-9

Braak, H., Rüb, U., Gai, W.P., Del Tredici, K., 2003a. Idiopathic Parkinson's disease: Possible routes by which vulnerable neuronal types may be subject to neuroinvasion by an unknown pathogen. J. Neural Transm. 110, 517–536. https://doi.org/10.1007/s00702-002-0808-2

Braak, H., Tredici, K., Rüb, U., Vos, R.A.I., Jansen Steur, E.N.H., Braak, E., 2003b. Staging of brain pathology related to sporadic Parkinson's disease. Neurobiol Aging 24, 197–211. https://doi.org/10.1016/S0197-4580(02)00065-9

Brown, P., 2006. Bad oscillations in Parkinson's disease, in: Journal of Neural Transmission, Supplement. Springer, Vienna , pp. 27–30. https://doi.org/10.1007/978-3-211-45295-0_6

Brown, P., Oliviero, A., Mazzone, P., Insola, A., Tonali, P., Di Lazzaro, V., 2001. Dopamine Dependency of Oscillations between Subthalamic Nucleus and Pallidum in Parkinson's Disease. J. Neurosci. 21, 1033–1038. https://doi.org/10.1523/JNEUROSCI.21-03-01033.2001

Brown, P., Williams, D., 2005. Basal ganglia local field potential activity: Character and functional significance in the human. Clin. Neurophysiol. https://doi.org/10.1016/j.clinph.2005.05.009

Burciu, R.G., Vaillancourt, D.E., 2018. Imaging of Motor Cortex Physiology in Parkinson's Disease. Mov. Disord. 33, 1688–1699. https://doi.org/10.1002/mds.102

Burré, J., 2015. The synaptic function of α-synuclein. J. Parkinsons. Dis.

https://doi.org/10.3233/JPD-150642

Burré, J., Sharma, M., Tsetsenis, T., Buchman, V., Etherton, M.R., Südhof, T.C., 2010. α-Synuclein promotes SNARE-complex assembly in vivo and in vitro. Science (80-.). 329, 1663–1667. https://doi.org/10.1126/science.1195227

Buzsáki, G., Anastassiou, C.A., Koch, C., 2012. The origin of extracellular fields and currents — EEG, ECoG, LFP and spikes. Nat Rev Neurosci 13, 407–420. https://doi.org/http://www.nature.com/nrn/journal/v13/n6/suppinfo/nrn3241_S1.html

Chandra, S., Fornai, F., Kwon, H.B., Yazdani, U., Atasoy, D., Liu, X., Hammer, R.E., Battaglia, G., German, D.C., Castillo, P.E., Südhof, T.C., 2004. Double-knockout mice for α- and β-synucleins: Effect on synaptic functions. Proc. Natl. Acad. Sci. U. S. A. 101, 14966–14971. https://doi.org/10.1073/pnas.0406283101

De Hemptinne, C., Swann, N.C., Ostrem, J.L., Ryapolova-Webb, E.S., San Luciano, M., Galifianakis, N.B., Starr, P.A., 2015. Therapeutic deep brain stimulation reduces cortical phase-amplitude coupling in Parkinson's disease. Nat. Neurosci. 18, 779–786. https://doi.org/10.1038/nn.3997

Doty, R.L., 2017. Olfactory dysfunction in neurodegenerative diseases: is there a common pathological substrate? Lancet Neurol. 16, 478–488. https://doi.org/https://doi.org/10.1016/S1474-4422(17)30123-0

Doty, R.L., 2012. Olfactory dysfunction in Parkinson disease. Nat. Rev. Neurol. 8, 329–339. https://doi.org/10.1038/nrneurol.2012.80

Doty, R.L., Ferguson-Segall, M., Lucki, I., Kreider, M., 1988. Effects of intrabulbar injections of 6-hydroxydopamine on ethyl acetate odor detection in castrate and non-castrate male rats. Brain Res 444, 95–103.

Doucette, W., Milder, J., Restrepo, D., 2007. Adrenergic modulation of olfactory bulb circuitry affects odor discrimination. Learn Mem 14, 539–547. https://doi.org/14/8/539 [pii]10.1101/lm.606407

Durante, V., de Iure, A., Loffredo, V., Vaikath, N., De Risi, M., Paciotti, S., Quiroga-Varela, A., Chiasserini, D., Mellone, M., Mazzocchetti, P., Calabrese, V.,

700 Campanelli, F., Mechelli, A., Di Filippo, M., Ghiglieri, V., Picconi, B., El-Agnaf, O.M.,
701 De Leonibus, E., Gardoni, F., Tozzi, A., Calabresi, P., 2019. Alpha-synuclein
702 targets GluN2A NMDA receptor subunit causing striatal synaptic dysfunction and
703 visuospatial memory alteration. Brain 142, 1365–1385.
704 https://doi.org/10.1093/brain/awz065

705 Eisinger, R.S., Cagle, J., Opri, E., Alcantara, J., Cernera, S., Foote, K.D., Okun, M.S.,
706 Gunduz, A., 2020. Parkinsonian beta dynamics during rest and movement in the
707 dorsal pallidum and subthalamic nucleus. J. Neurosci. 40, 2859–2867.
708 https://doi.org/10.1523/JNEUROSCI.2113-19.2020

709 Feingold, J., Gibson, D.J., DePasquale, B., Graybiel, A.M., 2015. Bursts of beta
710 oscillation differentiate postperformance activity in the striatum and motor cortex of
711 monkeys performing movement tasks. Proc. Natl. Acad. Sci. 112, 13687 LP –
712 13692. https://doi.org/10.1073/pnas.1517629112

713 Fujiwara, H., Hasegawa, M., Dohmae, N., Kawashima, A., Masliah, E., Goldberg, M.S.,
714 Shen, J., Takio, K., Iwatsubo, T., 2002. α-Synuclein is phosphorylated in
715 synucleinopathy lesions. Nat. Cell Biol. 4, 160–164. https://doi.org/10.1038/ncb748

716 Gadziola, M.A., Tylicki, K.A., Christian, D.L., Wesson, D.W., 2015. The Olfactory
717 Tubercle Encodes Odor Valence in Behaving Mice. J. Neurosci. 35, 4515–4527.
718 https://doi.org/10.1523/JNEUROSCI.4750-14.2015

719 Gervais, R., Buonviso, N., Martin, C., Ravel, N., 2007. What do electrophysiological
720 studies tell us about processing at the olfactory bulb level? J. Physiol. Paris 101,
721 40–45. https://doi.org/10.1016/j.jphysparis.2007.10.006

722 Giannicola, G., Marceglia, S., Rossi, L., Mrakic-Sposta, S., Rampini, P., Tamma, F.,
723 Cogiamanian, F., Barbieri, S., Priori, A., 2010. The effects of levodopa and ongoing
724 deep brain stimulation on subthalamic beta oscillations in Parkinson's disease. Exp.
725 Neurol. 226, 120–127. https://doi.org/10.1016/j.expneurol.2010.08.011

726 Goedert, M., 2001. Alpha-synuclein and neurodegenerative diseases. Nat Rev Neurosci
727 2. https://doi.org/10.1038/35081564

728 Gottfried, J.A., 2010. Central mechanisms of odour object perception. Nat Rev Neurosci
729 11, 628–641.
730 https://doi.org/http://www.nature.com/nrn/journal/v11/n9/suppinfo/nrn2883_S1.html

731 Haegens, S., Zion Golumbic, E., 2018. Rhythmic facilitation of sensory processing: A
732 critical review. Neurosci. Biobehav. Rev. 86, 150–165.
733 https://doi.org/https://doi.org/10.1016/j.neubiorev.2017.12.002

734 Hammond, C., Bergman, H., Brown, P., 2007. Pathological synchronization in
735 Parkinson's disease: networks, models and treatments. Trends Neurosci.
736 https://doi.org/10.1016/j.tins.2007.05.004

737 Kay, L.M., Beshel, J., 2010. A beta oscillation network in the rat olfactory system during
738 a 2-alternative choice odor discrimination task. J. Neurophysiol. 104, 829–839.

739 Kay, L.M., Beshel, J., Brea, J., Martin, C., Rojas-Líbano, D., Kopell, N., 2009. Olfactory
740 oscillations: the what, how and what for. Trends Neurosci. 32, 207–214.

741 Kay, L.M., Stopfer, M., 2006. Information processing in the olfactory systems of insects
742 and vertebrates. Semin. Cell Dev. Biol. 17, 433–442.
743 https://doi.org/http://dx.doi.org/10.1016/j.semcdb.2006.04.012

744 Komisaruk, B.R., 1970. Synchrony between limbic system theta activity and rhythmical
745 behavior in rats. J Comp Physiol Psychol 70, 482–492.

746 Kopell, N., Ermentrout, G.B., Whittington, M.A., Traub, R.D., 2000. Gamma rhythms and
747 beta rhythms have different synchronization properties. Proc. Natl. Acad. Sci. U. S.
748 A. 97, 1867–1872.

749 Kühn, A.A., Kupsch, A., Schneider, G.H., Brown, P., 2006. Reduction in subthalamic 8-
750 35 Hz oscillatory activity correlates with clinical improvement in Parkinson's
751 disease. Eur. J. Neurosci. 23, 1956–1960. https://doi.org/10.1111/j.1460-
752 9568.2006.04717.x

753 Lee, E.Y., Eslinger, P.J., Du, G., Kong, L., Lewis, M.M., Huang, X., 2014. Olfactory-
754 related cortical atrophy is associated with olfactory dysfunction in Parkinson's
755 disease. Mov. Disord. 29, 1205–1208. https://doi.org/10.1002/mds.25829

Little, S., Brown, P., 2014. The functional role of beta oscillations in Parkinson's disease. Park. Relat. Disord. 20, S44–S48. https://doi.org/10.1016/S1353-8020(13)70013-0

Lowry, C.A., Kay, L.M., 2007. Chemical factors determine olfactory system beta oscillations in waking rats. J Neurophysiol 98, 394–404. https://doi.org/00124.2007 [pii]10.1152/jn.00124.2007

Luk, K., Kehm, V., Zhang, B., O'Brien, P., Trojanowski, J., Lee, V., 2012. Intracerebral inoculation of pathological α-synuclein initiates a rapidly progressive neurodegenerative α-synucleinopathy in mice. J Exp Med 209. https://doi.org/10.1084/jem.20112457

Luk, K.C., Lee, V.M.-Y., 2014. Modeling Lewy pathology propagation in Parkinson's disease. Parkinsonism Relat. Disord. 20, S85–S87. https://doi.org/10.1016/S1353-8020(13)70022-1

Luk, K.C., Song, C., O'Brien, P., Stieber, A., Branch, J.R., Brunden, K.R., Trojanowski, J.Q., Lee, V.M.Y., 2009. Exogenous α-synuclein fibrils seed the formation of Lewy body-like intracellular inclusions in cultured cells. Proc. Natl. Acad. Sci. U. S. A. 106, 20051–20056. https://doi.org/10.1073/pnas.0908005106

Mahlknecht, P., Seppi, K., Poewe, W., 2015. The concept of prodromal Parkinson's disease. J. Parkinsons. Dis. https://doi.org/10.3233/JPD-150685

Martin, C., Beshel, J., Kay, L.M., 2007. An olfacto-hippocampal network is dynamically involved in odor-discrimination learning. J Neurophysiol 98, 2196–2205.

Mason, D.M., Nouraei, N., Pant, D.B., Miner, K.M., Hutchison, D.F., Luk, K.C., Stolz, J.F., Leak, R.K., 2016. Transmission of α-synucleinopathy from olfactory structures deep into the temporal lobe. Mol. Neurodegener. 11, 49. https://doi.org/10.1186/s13024-016-0113-4

McCarthy, M.M., Moore-Kochlacs, C., Gu, X., Boyden, E.S., Han, X., Kopell, N., 2011. Striatal origin of the pathologic beta oscillations in Parkinson's disease. Proc. Natl. Acad. Sci. U. S. A. 108, 11620–11625. https://doi.org/10.1073/pnas.1107748108

784 Mezias, C., Rey, N., Brundin, P., Raj, A., 2020. Neural connectivity predicts spreading
785 of alpha-synuclein pathology in fibril-injected mouse models: Involvement of
786 retrograde and anterograde axonal propagation. Neurobiol. Dis. 134, 104623.
787 https://doi.org/10.1016/j.nbd.2019.104623

788 Mitzdorf, U., 1985. Current source-density method and application in cat cerebral
789 cortex: investigation of evoked potentials and EEG phenomena. Physiol. Rev. 65,
790 37–100.

791 Moran, A., Bergman, H., Israel, Z., Bar-Gad, I., 2008. Subthalamic nucleus functional
792 organization revealed by parkinsonian neuronal oscillations and synchrony. Brain
793 131, 3395–409. https://doi.org/10.1093/brain/awn270

794 Morris, M., Sanchez, P.E., Verret, L., Beagle, A.J., Guo, W., Dubal, D., Ranasinghe,
795 K.G., Koyama, A., Ho, K., Yu, G.Q., Vossel, K.A., Mucke, L., 2015. Network
796 dysfunction in α-synuclein transgenic mice and human Lewy body dementia. Ann.
797 Clin. Transl. Neurol. 2, 1012–1028. https://doi.org/10.1002/acn3.257

798 Neville, K.R., Haberly, L.B., 2003. Beta and gamma oscillations in the olfactory system
799 of the urethane-anesthetized rat. J Neurophysiol 90, 3921–3930.

800 Nusser, Z., Kay, L.M., Laurent, G., Homanics, G.E., Mody, I., 2001. Disruption of
801 GABA(A) receptors on GABAergic interneurons leads to increased oscillatory
802 power in the olfactory bulb network. J Neurophysiol 86, 2823–2833.

803 Paxinos, G., Franklin, K., 2000. The Mouse Brain in Stereotaxic Coordinates, 2nd ed.
804 Academic Press, San Diego.

805 Peelaerts, W., Bousset, L., Baekelandt, V., Melki, R., 2018. α-Synuclein strains and
806 seeding in Parkinson's disease, incidental Lewy body disease, dementia with Lewy
807 bodies and multiple system atrophy: similarities and differences. Cell Tissue Res.
808 https://doi.org/10.1007/s00441-018-2839-5

809 Polinski, N.K.., Volpicelli-Daley, L.A.., Sortwell, C.E.., Luk, K.C.., Cremades, N., Gottler,
810 L.M.., Froula, J., Duffy, M.F.., Lee, V.M.., Martinez, T.N.., Dave, K.D.., 2018. Best
811 Practices for Generating and Using Alpha-Synuclein Pre-Formed Fibrils to Model

Parkinson's Disease in Rodents. J. Parkinsons. Dis.

Rall, W., Shepherd, G.M., 1968. Theoretical reconstruction of field potentials and dendrodendritic synaptic interactions in olfactory bulb. J Neurophysiol 31, 884–915.

Rey, N.L., George, S., Steiner, J.A., Madaj, Z., Luk, K.C., Trojanowski, J.Q., Lee, V.M.-Y., Brundin, P., 2018a. Spread of aggregates after olfactory bulb injection of α-synuclein fibrils is associated with early neuronal loss and is reduced long term. Acta Neuropathol. 135, 65–83. https://doi.org/10.1007/s00401-017-1792-9

Rey, N.L., Petit, G.H., Bousset, L., Melki, R., Brundin, P., 2013. Transfer of human α-synuclein from the olfactory bulb to interconnected brain regions in mice. Acta Neuropathol. 126, 555–573. https://doi.org/10.1007/s00401-013-1160-3

Rey, N.L., Steiner, J.A., Maroof, N., Luk, K.C., Madaj, Z., Trojanowski, J.Q., Lee, V.M.-Y., Brundin, P., 2016. Widespread transneuronal propagation of α-synucleinopathy triggered in olfactory bulb mimics prodromal Parkinson's disease. J. Exp. Med. 213, 1759–78. https://doi.org/10.1084/jem.20160368

Rey, N.L., Wesson, D.W., Brundin, P., 2018b. The olfactory bulb as the entry site for prion-like propagation in neurodegenerative diseases. Neurobiol. Dis. 109, 226–248. https://doi.org/http://dx.doi.org/10.1016/j.nbd.2016.12.013

Ross, G.W., Petrovitch, H., Abbott, R.D., Tanner, C.M., Popper, J., Masaki, K., Launer, L., White, L.R., 2008. Association of olfactory dysfunction with risk for future Parkinson's disease. Ann. Neurol. 63, 167–173. https://doi.org/10.1002/ana.21291

Schindelin, J., Arganda-Carreras, I., Frise, E., Kaynig, V., Longair, M., Pietzsch, T., Preibisch, S., Rueden, C., Saalfeld, S., Schmid, B., Tinevez, J.Y., White, D.J., Hartenstein, V., Eliceiri, K., Tomancak, P., Cardona, A., 2012. Fiji: An open-source platform for biological-image analysis. Nat. Methods. https://doi.org/10.1038/nmeth.2019

Schoppa, N.E., Urban, N.N., 2003. Dendritic processing within olfactory bulb circuits. Trends Neurosci 26, 501–506.

Scott, J.W., McBride, R.L., Schneider, S.P., 1980. The organization of projections from

840 the olfactory bulb to the piriform cortex and olfactory tubercle in the rat. J Comp
841 Neurol 194, 519–534.

842 Shepherd, G.M., 1972. Synaptic organization of the mammalian olfactory bulb. Physiol.
843 Rev. https://doi.org/10.1152/physrev.1972.52.4.864

844 Spillantini, M.G., Schmidt, M.L., Lee, V.M., Trojanowski, J.Q., Jakes, R., Goedert, M.,
845 1997. Alpha-synuclein in Lewy bodies. Nature 388. https://doi.org/10.1038/42166

846 Spitzer, B., Haegens, S., 2017. Beyond the Status Quo: A Role for Beta Oscillations in
847 Endogenous Content (Re)Activation. eneuro 4, ENEURO.0170-17.2017.
848 https://doi.org/10.1523/ENEURO.0170-17.2017

849 Spitzer, B., Wacker, E., Blankenburg, F., 2010. Oscillatory correlates of vibrotactile
850 frequency processing in human working memory. J. Neurosci. 30, 4496–4502.
851 https://doi.org/10.1523/JNEUROSCI.6041-09.2010

852 van Ede, F., Jensen, O., Maris, E., 2010. Tactile expectation modulates pre-stimulus A-
853 band oscillations in human sensorimotor cortex. Neuroimage 51, 867–876.
854 https://doi.org/10.1016/j.neuroimage.2010.02.053

855 Volpicelli-Daley, L.A., Luk, K.C., Lee, V.M.-Y., 2014. Addition of exogenous α-synuclein
856 preformed fibrils to primary neuronal cultures to seed recruitment of endogenous α-
857 synuclein to Lewy body and Lewy neurite–like aggregates. Nat. Protoc. 9, 2135.

858 Volpicelli-Daley, L.A., Luk, K.C., Patel, T.P., Tanik, S.A., Riddle, D.M., Stieber, A.,
859 Meaney, D.F., Trojanowski, J.Q., Lee, V.M.-Y., 2011. Exogenous α-synuclein fibrils
860 induce Lewy body pathology leading to synaptic dysfunction and neuron death.
861 Neuron 72, 57–71. https://doi.org/10.1016/j.neuron.2011.08.033

862 Wachowiak, M., Shipley, M.T., 2006. Coding and synaptic processing of sensory
863 information in the glomerular layer of the olfactory bulb. Semin Cell Dev Biol 17,
864 411–423.

865 Wattendorf, E., Welge-Lussen, A., Fiedler, K., Bilecen, D., Wolfensberger, M., Fuhr, P.,
866 Hummel, T., Westermann, B., 2009. Olfactory Impairment Predicts Brain Atrophy in
867 Parkinson's Disease. J. Neurosci. 29, 15410–15413.

868 https://doi.org/10.1523/jneurosci.1909-09.2009

869 Wen, M.C., Xu, Z., Lu, Z., Chan, L.L., Tan, E.K., Tan, L.C.S., 2017. Microstructural
870 network alterations of olfactory dysfunction in newly diagnosed Parkinson's
871 disease. Sci. Rep. 7, 12559. https://doi.org/10.1038/s41598-017-12947-7

872 Wilson, D.A., 2001. Scopolamine enhances generalization between odor
873 representations in rat olfactory cortex. Learn Mem 8, 279–285.

874 Wilson, D.A., Sullivan, R.M., 2011. Cortical processing of odor objects. Neuron 72, 506–
875 519.

876 Wu, Q., Takano, H., Riddle, D.M., Trojanowski, J.Q., Coulter, D.A., Lee, V.M.-Y., 2019.
877 Alpha-synuclein (αSyn) preformed fibrils induce endogenous αSyn aggregation,
878 compromise synaptic activity and enhance synapse loss in cultured excitatory
879 hippocampal neurons. J. Neurosci. 0060–19.
880 https://doi.org/10.1523/JNEUROSCI.0060-19.2019

881 Wu, X., Yu, C., Fan, F., Zhang, K., Zhu, C., Wu, T., Li, K., Chan, P., 2011. Correlation
882 between Progressive Changes in Piriform Cortex and Olfactory Performance in
883 Early Parkinson's Disease. Eur. Neurol. 66, 98–105.
884 https://doi.org/10.1159/000329371

885

Kulkarni et al., Figure 1

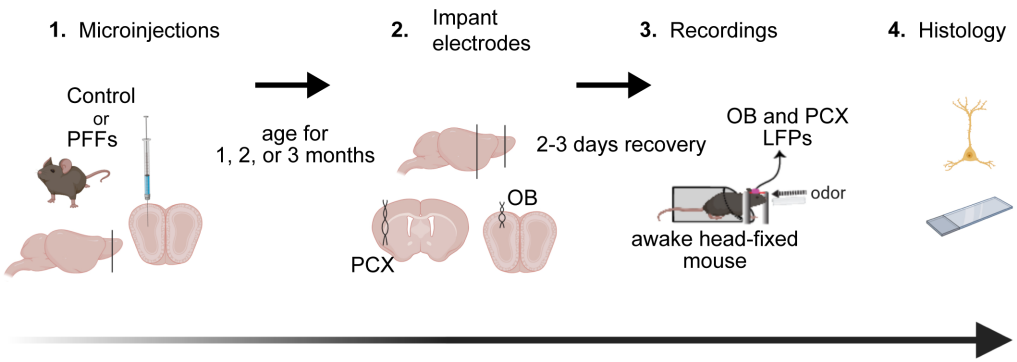

Fig 1. Experimental design for α-Syn seeding and subsequent multi-site LFP recordings in awake mice. 2-3 months old C57BL/6J mice received unilateral OB injections of either α-Syn PFFs or PBS and were aged for 1, 2, or 3 months post injection. The mice were then surgically implanted ipsilaterally to the initial surgical site in the OB and PCX with twisted bipolar electrodes for LFP recordings. Following this, the mice were allowed 2-3 days to recover. Spontaneous and odor-evoked LFPs were recorded from awake mice while they were head fixed (to allow control for the positioning of the snout relative to the odor port) in the absence and presence of odors respectively, and then were perfused within 3 days for *post-mortem* histology.

Kulkarni et al., Figure 2

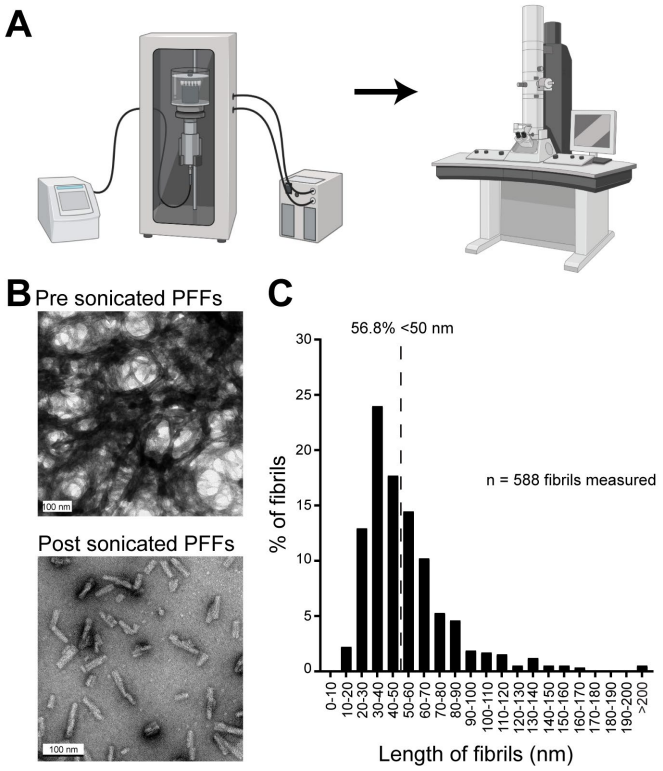

Fig 2. Verification of PFF length prior to OB injections. A, Experimental design, including sonication and electron microscopy, to optimize the length of the PFFs. **B,** Transmission electron microscopy images of PFFs before and after sonication. Scale bar represents 100 nm. **C,** Histogram of PFF length post sonication illustrating that >50% of the fibril population are <50 nm. Dashed line represents 50% of total population of PFFs quantified. Data from two separate sonication runs, 6-7 electron micrographs each.

Kulkarni et al., Figure 3

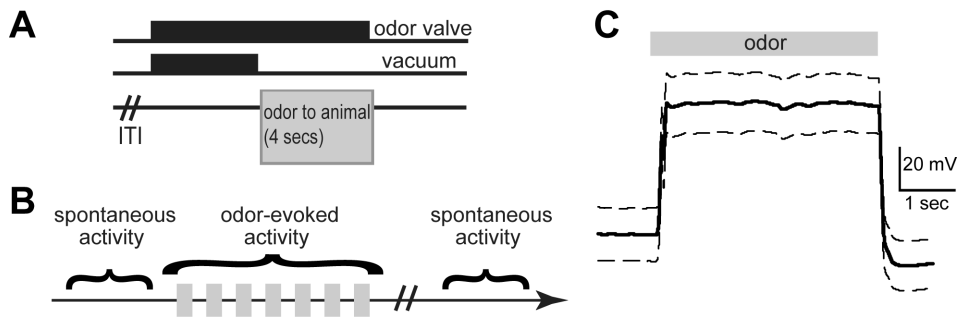

Fig 3. Paradigm for recording spontaneous and odor-evoked LFPs from head-fixed awake mice. A, After a variable inter-trial interval (ITI), the odor valves are turned on for 8 secs and the vacuum for 4 secs. This allows the animal to be presented with an odor for 4 secs. **B,** Schematic showing the recording paradigm. An epoch of spontaneous LFP activity was recorded before and after odor presentation. During odor presentation, 7 odors were presented in a pseudo-random order for 4-5 sessions, and their odor-evoked activity recorded. **C,** Average photoionization detector trace in response to 12 presentations of 1 Torr isopentyl acetate, depicting the rapid temporal dynamics and stability of odor presentation (10 Hz, low pass filtered). Data are mean +/- SEM.

Kulkarni et al., Figure 4

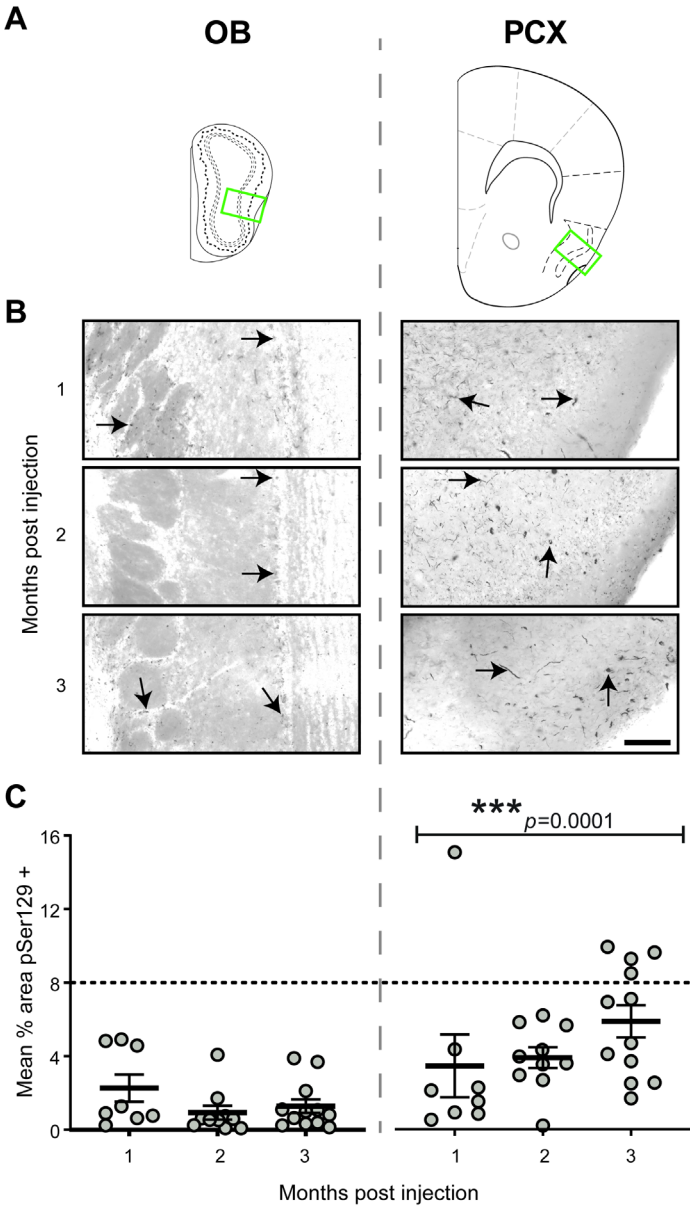

Fig 4. PFFs injected in the OB induced an amplification and spread of pathology to interconnected regions, including the PCX. Pser129 immunofluorescence was used as an assay to detect pathological α-Syn. **A,** Coronal panel showing the regions (green boxes) used for quantifying Pser129 expression level in the OB and PCX of mice injected with PFFs. **B,** Representative images of Pser129 immunofluorescence staining of the OB and PCX of mice aged for 1, 2, or 3 months post PFF seeding. Arrowheads in the OB and PCX panels indicate areas of neuritic pathology. **C,** Quantification of mean % area in all three brain regions, showing Pser129 immunofluorescence in PFF injected mice aged for 1 (n= 8), 2 (n= 10), and 3 (n= 12) months post injection. Significant increase in mean % area Pser129 was observed in the PCX when compared to the OB. ***$p \leq 0.001$ ANOVA followed by Tukey's multiple comparison's test.

Kulkarni et al., Figure 5

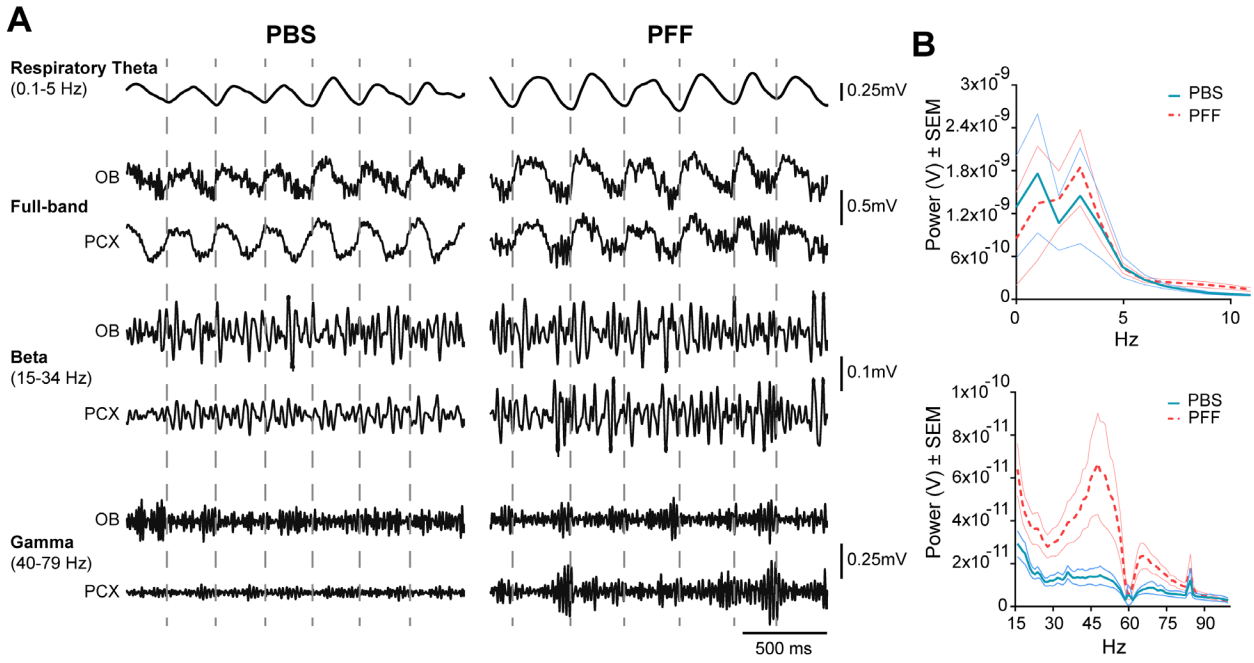

Fig 5. Aberrant transient spontaneous LFP activity in the PCX. A, Representative spontaneous LFP traces from two separate mice injected with either PBS (left) or PFF (right), 2 months prior to recording. Shown are full band traces from simultaneous OB and PCX recordings (0.1-100Hz) which were also filtered to separately display beta and gamma band activity as defined in the figure. Respiratory theta from the OB is also displayed along with dashed vertical lines indicating the timing of OB respiratory cycles for visual aid. **B,** Spontaneous PCX power spectrograms of theta (top), and beta and gamma spectral power (bottom) of PBS (n = 9) and PFF injected mice (n = 10) aged for 2 months post injection.

Kulkarni et al., Figure 6

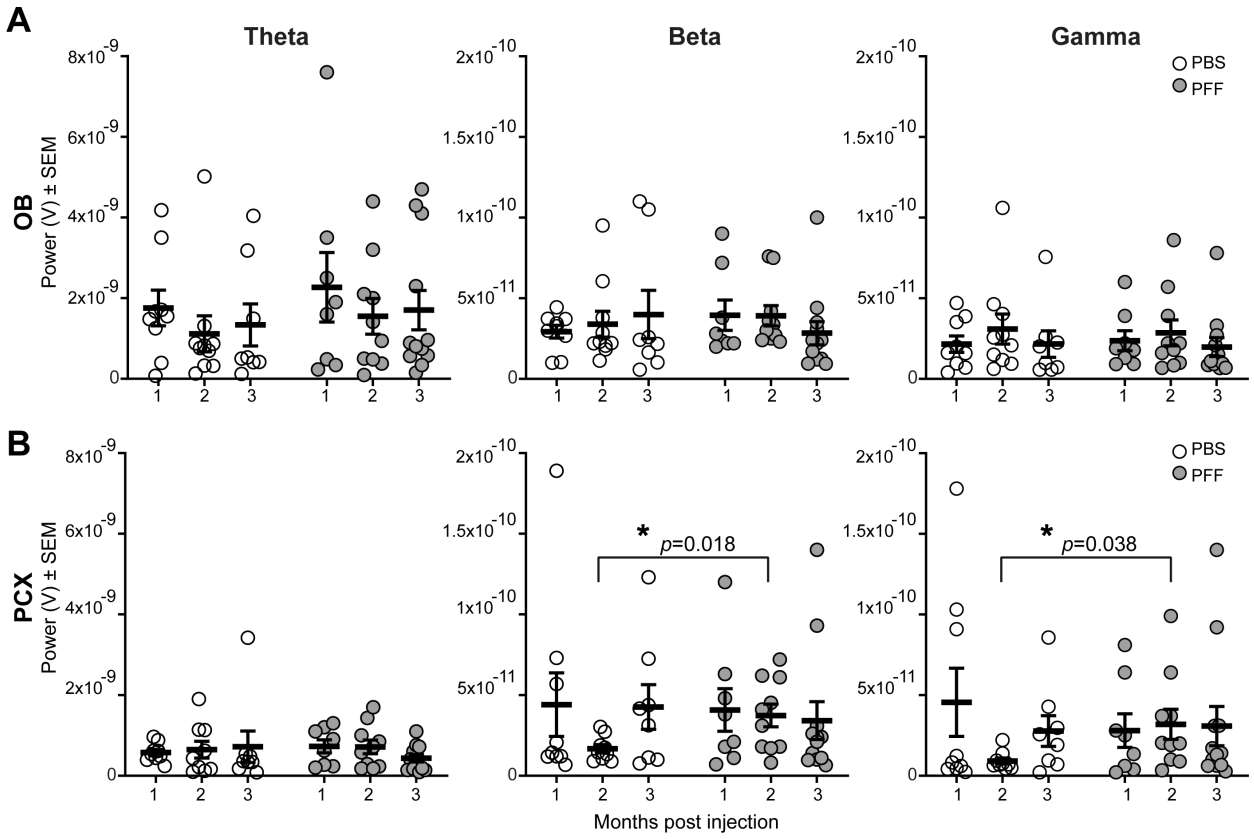

Fig 6. Quantification of spontaneous LFP activity reveals effects of PFF seeding in the PCX beta and gamma spectral bands. A,B, Spontaneous OB and PCX LFP power, consisting of theta (1-10 Hz), beta (15-34 Hz), and gamma (40-75 Hz) spectral bands in either PFF seeded mice or PBS injected mice aged for 1 (PFF: *n*= 8, PBS: *n*= 9), 2 (PFF: *n*= 10 , PBS: *n*= 9) , or 3 (PFF: *n*=12, PBS: *n*=8) months post injection. No treatment or age-post injection effect was observed in any of the cohorts. However, *post hoc* tests revealed a significant elevation in the beta and gamma band powers in the PCX of the 2 months group, age-matched PBS versus PFF. *ANOVA followed by two-tailed *t*-test.

Kulkarni et al., Figure 7

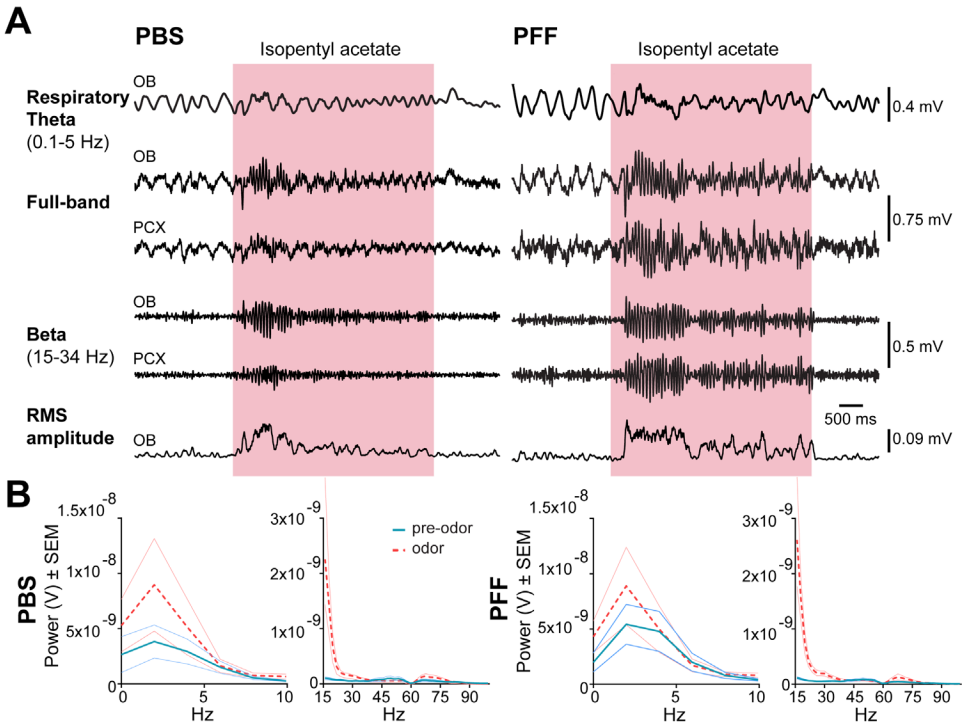

Fig 7. OB PFF seeding entails heightened odor-evoked OB beta band power. A, Representative odor-evoked LFP traces from two separate mice injected with either PBS (left) or PFF (right), 2 months prior to recording. Shown are full band traces from odor-evoked OB and PCX recordings (0.1-100Hz) which were also filtered to separately display beta band activity as defined in the figure. Respiratory theta from the OB is also displayed as is the root mean square of the beta band activity to illustrate elevated power of beta activity in the PFF injected versus PBS injected mouse. Pink shaded boxes indicate the time of odor delivery. **B,** Odor-evoked OB power spectrograms in the theta, and beta and gamma spectral bands of PBS (*n*= 9) and PFF injected mice (*n*= 10) aged for 2 months post injection.

Kulkarni et al., Figure 8

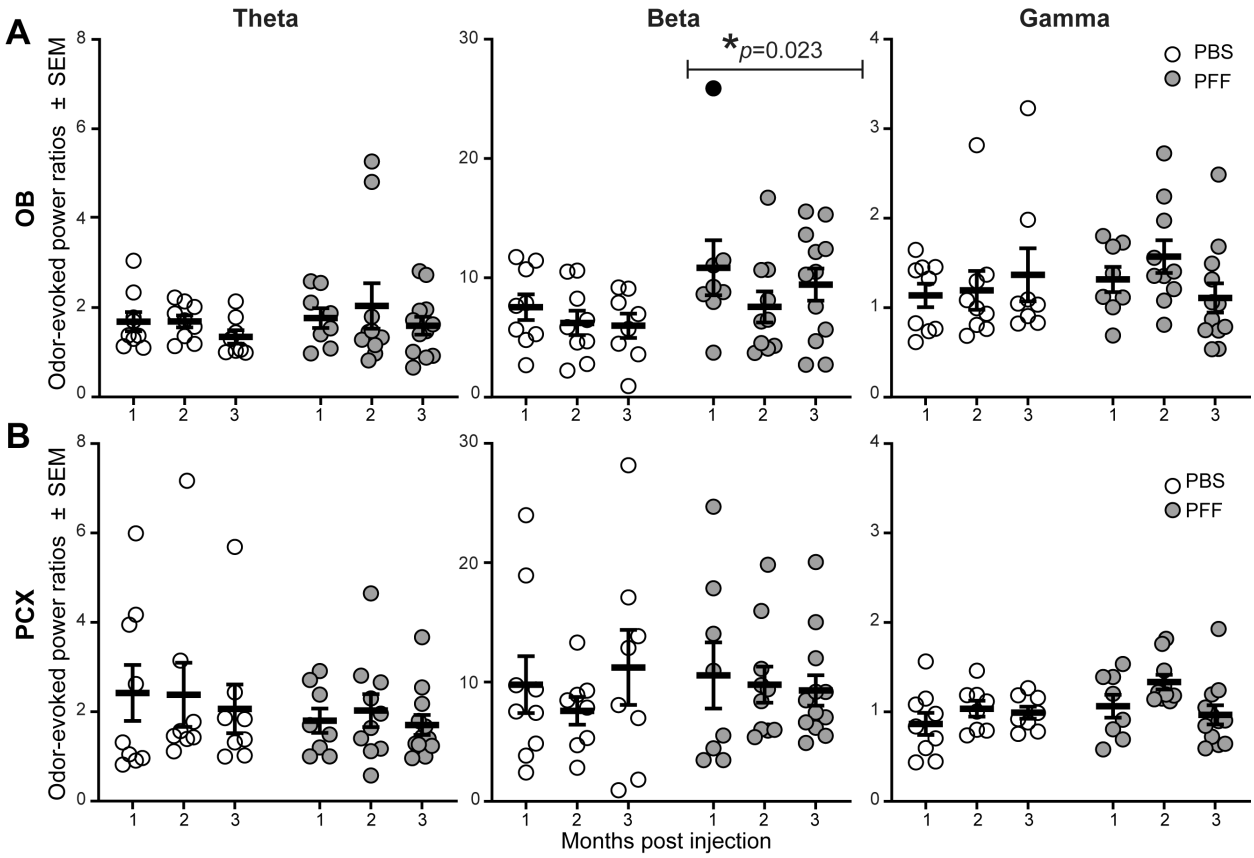

Fig 8. Analyses of odor-evoked activity uncovers PFF seeding induced aberrant OB beta band power during odor. A,B, Odor-evoked OB and PCX LFP power, consisting of theta (1-10 Hz), beta (15-34 Hz), and gamma (40-75 Hz) spectral bands in either PFF seeded mice or PBS injected mice aged for 1 (PFF: *n*= 8, PBS: *n*= 9), 2 (PFF: *n*= 10 , PBS: *n*= 9), or 3 (PFF: *n*=12, PBS: *n*=8) months post injection. Across all age groups, a significant increase in the beta band power in the OB of PFF seeded mice was observed when compared to PBS treated. *ANOVA. Solid data point indicates an animal whose elevated OB beta power associated with high OB Pser129 pathological burden.

Kulkarni et al., Figure 9

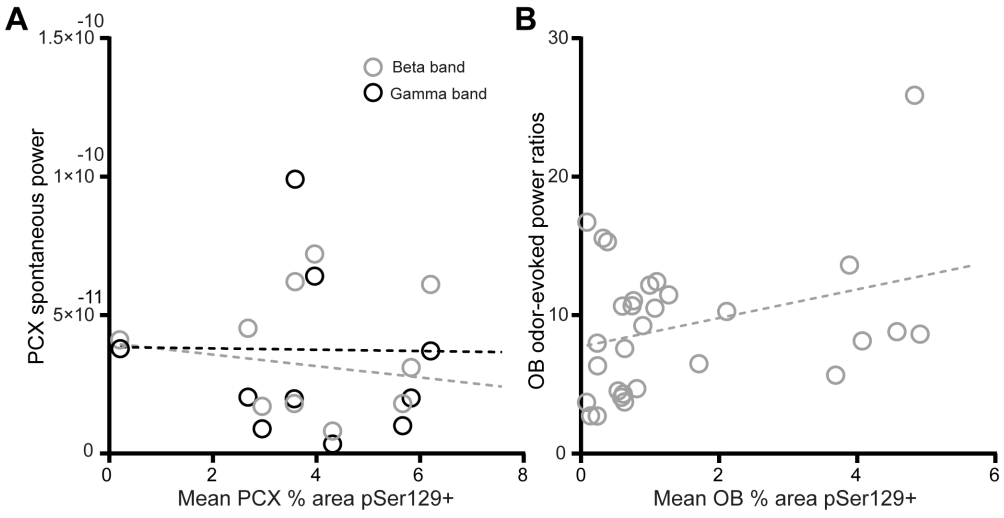

Fig 9. Lack of statistical correlation between Pser129 burden and aberrant LFP dynamics. A, Scatterplot illustrating the relationship between the mean % area occupied by Pser129 in the PCX (as quantified in **Fig. 4**) and beta (gray, 15-34 Hz) and gamma band spontaneous PCX activities (black, 40-75 Hz). Gray and black dashed lines indicate the linear fit for beta (r^2 = 0.0004) and gamma band (r^2 = 0.016) data sets respectively. **B,** Scatterplot illustrating the relationship between the mean % area occupied by Pser129 in the OB (as quantified in **Fig. 4**) and odor-evoked beta power (gray, 15-34 Hz). Gray dashed line indicates the linear fit (r^2 = 0.102).